Triangular and Rectangular Lattices for Cosecant-Squared-Shaped Beam Reflectarrays

Kendrick Q. Henderson, *Student Member, IEEE*, and Nima Ghalichechian, *Senior Member, IEEE*

***Abstract*—In this letter, we design, analyze, simulate, fabricate, and measure the performance of reflectarrays capable of forming cosecant-squared beam shape. Due to their unique pattern and abrupt change, achieving a cosecant-squared beam is challenging. In our effort, we evaluate the efficacy of a commonly used rectangular lattice and compare it, for the first time, to a triangular lattice. Two linearly polarized reflectarrays, each with 20 λ_0 diameter in size, are fabricated and tested at 20 GHz. Through statistical methods, we quantify the gain agreement between the desired cosecant-squared mask and the measured beam patterns for both rectangular and triangular lattices. We have found that the rectangular lattice conforms better to the cosecant-squared mask at the design frequency of 20 GHz with a root-mean-square error of 6.27 dB. The triangular lattice conforms less, however, it does allow for an increase in gain bandwidth of 6.2% as compared to 4.5% for the rectangular lattice. Measured and simulated patterns are in a good agreement.**

***Index Terms*—Beam shaping, cosecant-squared, lattice, rectangular, reflectarray, triangular.**

I. Introduction

REFLECTARRAY antennas are a low-profile, lightweight, and planar high-gain alternative to the conventional large and bulky parabolic reflectors. Unlike phased array antennas, which require a complex feed network, reflectarrays combine many of the features of the aforementioned conventional solutions. As such, the feed network is no longer required. A reflectarray is a discretized aperture of unit-cell elements that are illuminated by a feed source. The purpose of the unit cells is to compensate for the spatial delay difference between the feed source and the unit cell's position in the array. Controlling the phase response of the unit cells allows for the formation and steering of a far-field radiation pattern. Unlike a shaped beam reflector that requires a surface gradient, this method of phase control allows the array to remain planar. It also ensures a much greater efficiency for the reflectarrays compared to phased arrays due to the lack of a feed network.

Reflectarrays are a versatile antenna type that combines many of the favorable traits of both reflectors and phased arrays while minimizing many of the drawbacks of the two. Consequently, reflectarrays are used in some of the same application areas such as radars and communications. During the operation, the transmitting and receiving antennas in these applications must create or steer unique beam patterns. Specifically, a cosecant-squared ($\csc^2\theta = \frac{1}{\sin^2\theta}$) pattern is desirable to enhance the radar performance by compensating for the free path loss for airborne targets. The beam pattern allows the radar to be scanned in azimuth to quickly spot targets at range. One important characteristic for a radar antenna of this type is its ability to track the desired beam shape over the required bandwidth. However, the algorithms used to create these beam patterns for reflectarrays usually assume that the individual radiating elements are independent of each other and are not coupled in either magnitude or phase [1]–[4]. This may result in distortion of the resulting radiation pattern in a full-wave solver using the desired radiating element [5], [6].

The most common technique used to counter the coupling effects of unit cells is to include the simulated scattering parameters of the cell into the optimization algorithm. An increase in computation time and complexity may result in additional disadvantages with little practical benefit however [7], [8]. A few cosecant-squared reflectarrays utilize the previously mentioned method despite its drawbacks [9], [10].

One unstudied method for reducing the aforementioned interelement coupling and improving pattern conformability involves the manipulation of the lattice of reflectarrays [11], [12]. Although proven useful for phased arrays, the use of this method for reflectarrays has yet to be truly explored. At the present time, few if any detailed comparisons of the effects of various lattice structures for measured reflectarrays have been published. This letter observes the effect of the triangular lattice upon the radiation pattern of a cosecant-squared reflectarray as compared to the commonly used rectangular lattice. The design of a reflectarray's aperture to optimize its performance for its intended performance can be a challenging endeavor. This letter studies the effect of two lattice types and validates our simulation with measured results. The results are compared statistically using root-mean-squared error (RMSE) and coefficient of determination (R^2). We build on our prior work with the design of a novel metal-only reflectarray with a pencil beam [13]

Manuscript received July 8, 2021; accepted August 1, 2021. Date of publication August 13, 2021; date of current version October 6, 2021. This work was supported in part by the Department of Defense SMART Fellowship Program, Naval Surface Warfare Center - Crane Division, and in part by the Ohio State Consortium on Electromagnetics and Radio Frequencies. *(Corresponding author: Nima Ghalichechian.)*

Kendrick Q. Henderson was with ElectroScience Laboratory, Department of Electrical and Computer Engineering, The Ohio State University, Columbus, OH 43212 USA. He is now with the Naval Surface Warfare Center – Crane Division, Crane, IN 47522 USA (e-mail: kendrick.q.henderson.civ@us.navy.mil).

Nima Ghalichechian was with the ElectroScience Laboratory, Department of Electrical and Computer Engineering, The Ohio State University, Columbus, OH 43212 USA. He is now with the School of Electrical and Computer Engineering, Georgia Institute of Technology, Atlanta, GA 30308 USA (e-mail: nima.1@gatech.edu).

Digital Object Identifier 10.1109/LAWP.2021.3103152

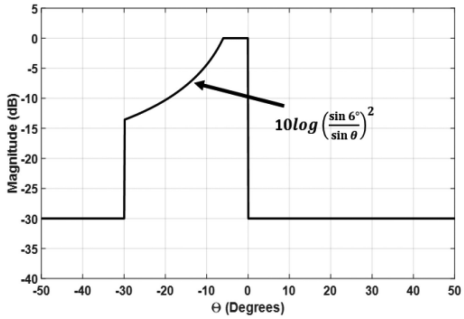

Fig. 1. Cosecant-squared far-field mask is defined as a desired pattern in azimuth plane.

TABLE I
PARAMETERS OF THE REFLECTARRAYS

Center Frequency	20 GHz
Horn Gain	15.9 dB
Horn Beamwidth	30°
Reflectarray Diameter	$20\lambda_0$ (300 mm)
Height-to-Diameter Ratio	0.9
Feed offset	15°
Feed Location (x, y, z)	0 mm, 84.3, 314.9 mm

and a mechanically steerable array [14]. The Gerchberg–Saxton algorithm is used to create near ideal cosecant-squared beam patterns in Section II. In Section III, multislot reflectarrays are characterized using full-wave simulation. The triangular and rectangular lattice reflectarrays are fabricated, measured, and analyzed in Section IV. Finally, Section V concludes this letter.

II. REFLECTARRAY DESIGN AND SIMULATION

For this letter, the Gerchberg–Saxton algorithm also known as Intersection Projection Method [1], [15] is used to determine the phases of a cosecant-squared beam pattern within the vertical plane of the reflectarrays. The algorithm uses a forward and backward projection between the reflectarray's aperture and far-field to optimize the phases of the reflectarray's unit cell with a maximum phase range of 360°. As shown in Fig. 1, the main cosecant-squared pattern starts at 6° and continues to 30°, with the sidelobe levels 30 dB below the main beam. This aggressive sidelobe level was chosen somewhat arbitrarily to evaluate how well the reflectarray could track the desired pattern. Table I lists the key parameters of the reflectarray. The feed location is chosen to maximize the reflectarray's aperture efficiency and to avoid aperture blockage.

Next, the rectangular and triangular lattices are defined for the two reflectarrays. For the rectangular lattice, the elements are spaced 0.5 λ_0 (λ_0 = free-space wavelength) apart in both the *x*- and *y*-axis. The shape of the rectangular lattice reflectarray used during optimization is shown in Fig. 2. For the triangular lattice, the pattern is constructed with the elements initially spaced similar to the rectangular lattice, whereas the odd number of rows is shifted laterally by 0.25 λ_0. The rectangular lattice has 1256 and the triangular lattice has 1197 elements. The triangular lattice is shown in Fig. 3. Initially, the far-field pattern is formed

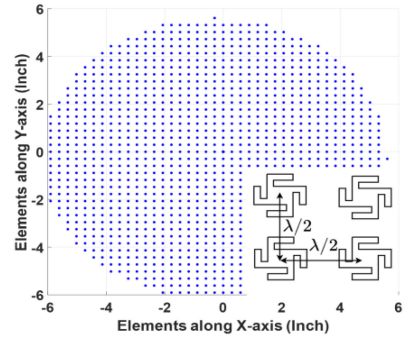

Fig. 2. Rectangular lattice used for the cosecant-squared reflectarray.

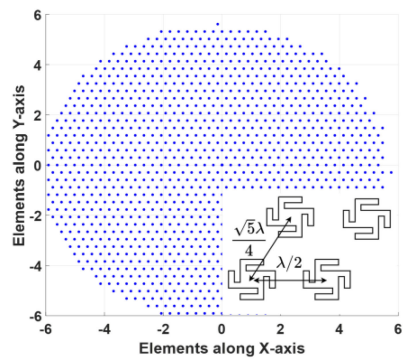

Fig. 3. Triangular lattice used for the cosecant-squared reflectarray.

as a pencil beam that is normal to the reflectarray surface and is then optimized toward the mask using the Gerchberg–Saxton algorithm. The RMSE (1) between the mask and optimized far-field was used to determine convergence. $M(\theta)$ is the mask and $A(\theta)$ is the optimized pattern in the equation. The maximum allowed number of iteration was 1000. To avoid local minima and traps, the simulated half-power beamwidth of the feed is very narrow in the initial part of the optimization and broaden in the final stage to 30°, similar to other works [1], [9]. The coefficient of determination in (2) is used as an additional method used for comparison of the final pattern to the mask

$$\mathrm{RMSE} = \sqrt{\int |M(\theta) - A(\theta)|^2 d\theta} \tag{1}$$

$$R^2 = 1 - \frac{\sum_i \left(A(\theta_i) - M(\theta_i)\right)^2}{\sum_i \left(A(\theta_i) - \overline{A(\theta)}\right)^2}. \tag{2}$$

For both reflectarrays, the results shown in Fig. 4 are identical and follow the mask well except at $\theta = -30$ and $\theta = 0$. This is expected, as the Gerchberg–Saxton excludes interelement coupling. We implemented two methods to quantify the closeness of the mask with our numerically calculated or later on with the measured patterns. For $-50 < \theta < 50$, RMSE is computed to be 8.06 dB and R^2 is 0.88. Both reflectarrays conform well within the main lobe of the mask with sidelobe level of –22 dB. The phase maps of both the triangular and rectanguar lattices are shown in Fig. 5.

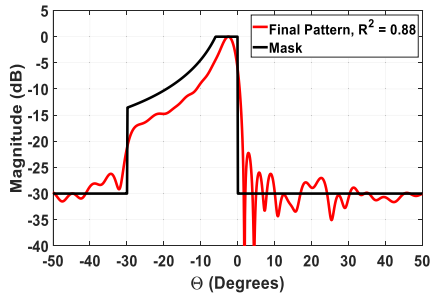

Fig. 4. Optimized computed far-field radiation in the azimuth plane is compared to the ideal mask.

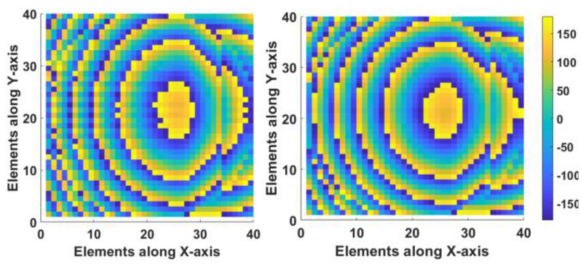

Fig. 5. Phase map of the triangular lattice on the left and the rectangular lattice on the right. The feed horn is on the left side of the plots.

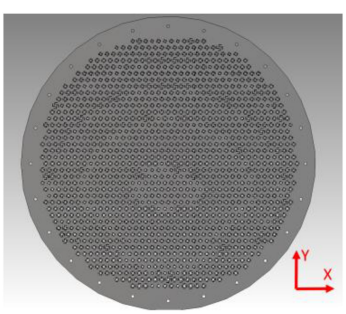

Fig. 6. Model of the triangular lattice reflectarray using the multislot element. Full-wave simulation is performed on this 20 λ_0 diameter array.

III. Full-Wave Simulation of Reflectarrays

The beamforming ability of both the rectangular and triangular lattice reflectarrays was analyzed using CST Studio Suite and the Integral Solver. To create the model of the reflectarrays, in-house automation software was used as the geometries of the multislot were too complex to create manually [13]. Fig. 6 illustrates the 20 λ_0 diameter model. The reflectarrays were excited using a *K*-band horn (Eravant SAC-1533-470-S2) with a 30° half-power beamwidth. To maximize the aperture efficiency and avoid feed blockage, the feed horn is placed at a focal length ratio of 0.9 and at an offset angle of 15°. The reflection coefficients of the rectangular and triangular lattices were 9 and 8.7 dB, respectively, at the design frequency of 20 GHz. A matching network could be designed to improve the impedance bandwidth but that is outside the scope of this letter. The purpose of this study was to investigate the effect of lattice of the beamforming ability of reflectarrays.

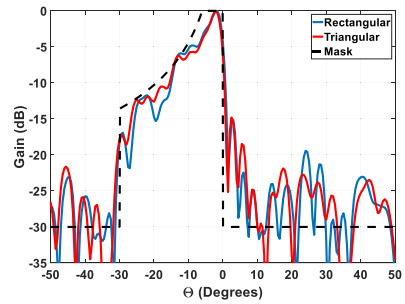

Fig. 7. Simulated cosecant-squared radiation patterns at 20 GHz for the rectangular and triangular reflectarrays. The arrays are *x*–*z* polarized.

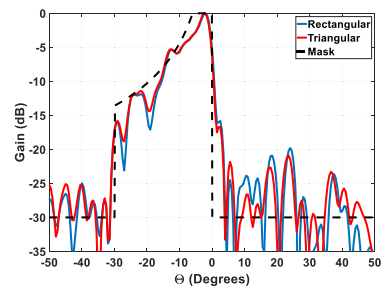

Fig. 8. Simulated cosecant-squared radiation patterns at 20 GHz for the rectangular and triangular reflectarrays. The arrays are *y*–*z* polarized.

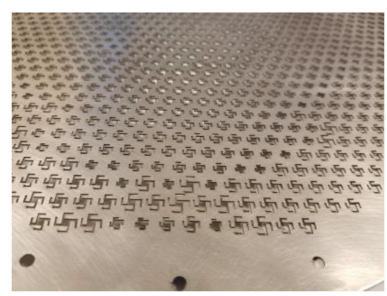

Fig. 9. Top surface of the fabricated cosecant-squared reflectarray with triangular lattice. The design frequency is 20 GHz.

The effect of the triangular and rectangular lattice was also investigated for both the *x*–*z* and *y*–*z* polarizations. A comparison of the *x*–*z* polarized far-fields of both lattices shown in Fig. 7 indicates that the triangular lattice performs better than the rectangular lattice in conforming to a desired far-field pattern. The RMSEs are 11.04 and 9.53 dB for the rectangular and triangular lattices, respectively. The two distinct nulls, at –27° and –20°, in the main lobe of the rectangular lattice radiation pattern indicate that the triangular lattice has a lower interelement coupling than the rectangular lattice. Note also in the other *y*–*z* polarization, the superior performance of the triangular lattice over the rectangular lattice as illustrated in Fig. 8.

IV. Fabrication and Measurement

To verify the coupling of both lattices, the simulated reflectarrays were fabricated and assembled. The elements of each reflectarray were laser-machined into the top stainless-steel surface, as shown in Fig. 9 (triangular lattice). A tolerance of 0.0245 mm

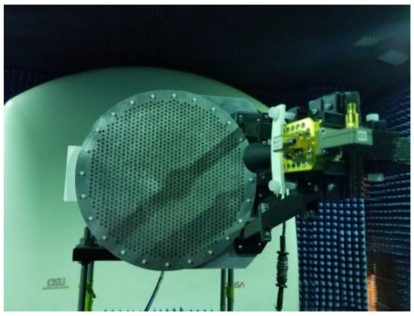

Fig. 10. Fabricated triangular lattice reflectarray mounted in the anechoic chamber for measurements.

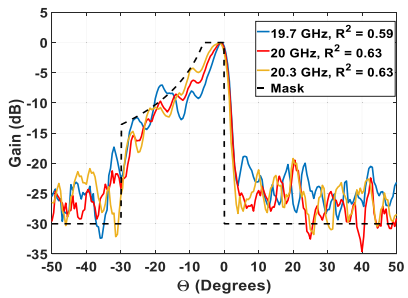

Fig. 11. Measured radiation pattern of the rectangular lattice reflectarray over 600 MHz of bandwidth from 19.7 to 20.3 GHz.

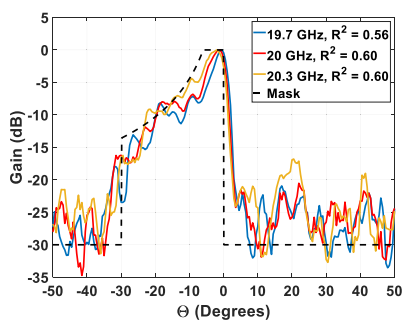

Fig. 12. Measured radiation pattern of the triangular lattice reflectarray over 600 MHz of bandwidth from 19.7 to 20.3 GHz.

(1 mil) for the laser etching process results in an average phase error of 4.3° over the 360° full tuning range of the multislot. At 20 GHz, this small phase error exhibits a minor effect on the gain patterns for the fully assembled reflectarrays. The balance of the components for the reflectarray (i.e., the ground plane with the height of 4 mm, rotator plate, dielectric spacers, and horn fixture) are similar to that used in our previous study [13].

The antennas were placed in the anechoic chamber at The Ohio State University, as shown in Fig. 10. The reflectarrays were then measured for the horizontal polarization given its indicator as the greatest difference between the two lattices. The measured results are first compared at the design frequency of 20 GHz. As shown in Fig. 11, the normalized gain patterns of the rectangular lattice exhibit a greater conformability to the desired mask than the triangular lattice of Fig. 12. The RMSEs were 6.27 and 6.49 dB for the rectangular and triangular lattices, respectively. Moreover, unlike the rectangular lattice, the main beam of the triangular lattice reflectarray keeps the desired shape

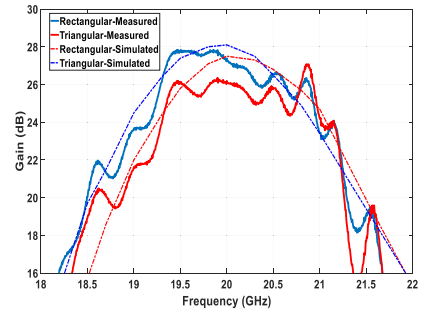

Fig. 13. Gain of both reflectarrays as a function of frequency.

up to 30°. The rectangular lattice does have a smoother gain response as compared to the triangular lattice.

The reflectarrays were also compared over 600 MHz of bandwidth from 19.7 to 20.3 GHz to capture the change in radiation patterns as a function of frequency. As shown in Fig. 11, the rectangular lattice reflectarray exhibits a greater degree of conformability to the desired mask, due to a higher element density along the plane from the equilateral distance of the lattice. The minimum and maximum RMSEs were 6.28 dB at 20.3 GHz and 6.56 dB at 19.7 GHz, respectively. Coupling becomes less of a problem at higher frequencies. As shown in Fig. 12, the triangular lattice reflectarray performs worse than the rectangular lattice as it reduces the interelement coupling but the number of elements that contribute to the beam pattern is reduced as well. The minimum and maximum RMSEs were 6.49 dB at 20 GHz and 6.80 dB at 19.7 GHz, respectively, across the band. The R^2 difference between the two lattices was consistently 3% over frequency. The peak gains at 20 GHz were 27.1 and 26 dB, respectively, for the rectangular and triangular lattices in Fig. 13. The respective gain bandwidths were 4.5% and 6.2% for the rectangular and triangular reflectarrays.

V. Conclusion

The purpose of this letter is to reduce the interelement coupling between the reflectarray elements for the cosecant-squared beams to improve conformability to the desired far-field mask. At the center frequency of 20 GHz, the rectangular lattice outperformed the triangular lattice in conforming to the cosecant-squared mask with a lower RMSE of 6.27 dB compared to 6.49 dB. The rectangular lattice conformed better over frequency as well characterized by a lower RMSE. Several deficiencies, however, characterize the triangular lattice. First, the peak gain of the triangular lattice reflectarray is lower than the rectangular lattice reflectarray. A difference of 1.1 dB in gain characterizes the horizontal polarization, which is the result of the decreased number of radiating elements for the triangular reflectarray and the overall asymmetry. The asymmetry of the triangular lattice would increase the axial ratio in applications that utilize circular polarization. In applications that require increased polarization purity, the asymmetric pattern of the lattice would be beneficial. The additional benefit of the triangular lattice is its ability to lower interelement coupling in reflectarrays. While the multislot element used in this study has a low average phase error of 4.3°, the reduced element count results less elements that could contribute to the formation of the cosecant-squared pattern.

REFERENCES

[1] J. A. Zornoza and J. A. Encinar, "Efficient phase-only synthesis of contoured-beam patterns for very large reflectarrays," *Int. J. RF Microw., Comput.-Aided Eng.*, vol. 14, no. 5, pp. 415–423, 2004.

[2] P. Nayeri, A. Z. Elsherbeni, and F. Yang, "Radiation analysis approaches for reflectarray antennas," *IEEE Antennas Propag. Mag.*, vol. 55, no. 1, pp. 127–134, Feb. 2013.

[3] O. M. Bucci, G. Franceschetti, G. Mazzarella, and G. Panariello, "Intersection approach to array pattern synthesis," *IEE Proc. H—Microw., Antennas Propag.*, vol. 137, no. 6, pp. 349–357, Dec. 1990.

[4] D. W. Boeringer and D. H. Werner, "Particle swarm optimization versus genetic algorithms for phased array synthesis," *IEEE Trans. Antennas Propag.*, vol. 52, no. 3, pp. 771–779, Mar. 2004.

[5] K. Karnati, S. Ebadi, and X. Gong, "Effects of inter-element spacing on mutual coupling and resonant properties in reflectarray unit cell design," in *Proc. IEEE Radio Wireless Symp.*, Santa Clara, CA, USA, 2012, pp. 83–86.

[6] K. K. Karnati, S. Ebadi, and X. Gong, "Dependency of Ka-band reflectarray unit cell reflection properties on the spacing between antenna elements," in *Proc. IEEE Radio Wireless Symp.*, Austin, TX, USA, 2013, pp. 118–120.

[7] A. Niccolai, R. Zich, M. Beccaria, and P. Pirinoli, "SNO based optimization for shaped beam reflectarray antennas," in *Proc. 13th Eur. Conf. Antennas Propag.*, Krakow, Poland, 2019, pp. 1–4.

[8] D. R. Prado, J. A. Lopez Fernandez, M. Arrebola, M. R. Pino, and G. Goussetis, "General framework for the efficient optimization of reflectarray antennas for contoured beam space applications," *IEEE Access*, vol. 6, pp. 72295–72310, 2018.

[9] G. Carluccio, A. Mazzinghi, and A. Freni, "Design and manufacture of cosecant-squared complementary reflectarrays for low-cost applications," *IEEE Trans. Antennas Propag.*, vol. 65, no. 10, pp. 5220–5227, Oct. 2017.

[10] Y. Pan, Y. R. Zhang, and X. Yu, "A X/Ku dual-band reflectarray design with cosecant squared shaped beam," *Microw., Opt. Technol. Lett.*, vol. 56, no. 9, pp. 2028–2034, 2014.

[11] O. Kiris, K. Topalli, and M. Unlu, "A reflectarray antenna using hexagonal lattice with enhanced beam steering capability," *IEEE Access*, vol. 7, pp. 45526–45532, 2019.

[12] M. W. Niaz, Z. Ahmed, and M. B. Ihsan, "Reflectarray with logarithmic spiral lattice of elementary antennas on its aperture," *AEU—Int. J. Electron. Commun.*, vol. 70, no. 8, pp. 1050–1054, 2016.

[13] K. Q. Henderson and N. Ghalichechian, "Circular-polarized metal-only reflectarray with multi-slot elements," *IEEE Trans. Antennas Propag.*, vol. 68, no. 9, pp. 6695–6703, Sep. 2020.

[14] K. Q. Henderson and N. Ghalichechian, "Steerable reflectarray using tunable height dielectric for high-power applications," in *Proc. 14th Eur. Conf. Antennas Propag.*, Copenhagen, Denmark, 2020, pp. 1–4.

[15] D. R. Prado, M. Arrebola, M. R. Pino, and F. Las-Heras, "Improved reflectarray phase-only synthesis using the generalized intersection approach with dielectric frame and first principle of equivalence," *Int. J. Antennas Propag.*, vol. 2017, pp. 1–11, 2017.